AIAA JOURNAL
Vol. 36, No. 9, September 1998

Measurement and Analysis of the Flowfields Induced by Suction Perforations

D. G. MacManus* and J. A. Eaton†
National University of Ireland, Galway, Ireland

The flow physics of laminar flow control suction surfaces is revealed by performing a detailed fundamental experimental investigation of an isolated suction perforation. A unique series of nonintrusive, high-resolution measurements are obtained using a three-component laser Doppler velocimetry system, and experiments are conducted in a low-speed, low-turbulence wind tunnel. The suction perforation flowfields are mapped for a range of sub- and supercritical suction rates and are found to be highly three dimensional. A rich variety of flowfield features is observed, including a pair of counter-rotating longitudinal vortices, multiple corotating longitudinal vortices, spanwise variations of the mean flow, and inherently unstable boundary-layer profiles. Critical suction limits, over a range of freestream speeds, are determined, and a new design criterion for critical suction is established. It is also shown that for sufficiently small perforations, irrespective of suction flow, boundary-layer transition does not occur. Further analyses of the measurements explore the possibility of interaction between the crossflow vortices and the suction-induced longitudinal vortices. The suction-induced transition process is discovered to commence with an instability of the longitudinal vortices. Engineering design criteria, i.e., suction limits and perforation spacings, are established.

Nomenclature

b_1	= spacing between vortex pair induced by an isolated suction perforation
b_2	= spacing between adjacent vortices produced by a row of perforations
d	= diameter of suction perforation
G_k	= Goldsmith's[10] sucked streamtube parameter, $(1/\nu)\,Q_h^{2/3}(\partial U/\partial y)\|_w^{1/3}$
L	= depth of suction perforation
M	= Mach number
$\dot{m}$	= mass flow rate through suction perforation
P_k	= roughness analogy transition parameter, $(y_k/\delta^*)\sqrt{Re_{\delta^*}}$
Q_h	= volume flow rate through suction perforation
Re_d	= suction Reynolds number, $V_h d/\nu$
Re_k	= streamtube Reynolds number, $U_k y_k/\nu$
Re_{δ^*}	= Reynolds number based on displacement thickness, $U_e\delta^*/\nu$
Re'	= unit Reynolds number, U_e/ν
s	= pitch of suction perforations
U, V, W	= mean velocities along x, y, and z, respectively
V_h	= average suction velocity through perforation, $Q_h/(\pi d^2/4)$
x, y, z	= Cartesian coordinates in streamwise, spanwise, and normal directions
y_k	= maximum height of sucked streamtube
z_k	= maximum width of sucked streamtube
δ	= thickness of boundary layer ($\delta_{99\%}$)
δ^*	= displacement thickness of unperturbed boundary layer
λ	= wavelength
ν	= kinematic viscosity

Subscripts

cf	= crossflow
crit	= critical value for transition
e	= edge of boundary layer
rms	= root mean square
w	= at the wall
∞	= freestream conditions

Received Sept. 18, 1997; revision received Jan. 12, 1998; accepted for publication May 22, 1998.

*Research Engineer, Aerospace Research Centre; currently Advanced Technologist, Turbine Systems, Rolls-Royce plc., P.O. Box 31, Derby DE24 8BJ, England, UK. Member AIAA.

†Director, Aerospace Research Centre. Senior Member AIAA.

I. Introduction

THE improvement of drag reduction techniques is a perennial objective of aircraft designers and manufacturers. Among the wide variety of techniques that have been explored, laminar flow control (LFC) may offer the greatest potential for drag reduction. LFC reduces the skin-friction drag, which accounts for up to 50% of total drag at cruise,[1] by stabilizing the boundary layer and moving the transition location as far aft as possible. This is not a trivial task, especially in light of the variety, sensitivity, interdependence, and complexity of the instability mechanisms that affect a laminar boundary layer under transonic flight conditions. Contemporary thinking suggests that for wing and tail surfaces the laminar boundary layer is best stabilized using hybrid laminar flow control (HLFC). HLFC consists of a combination of surface suction, applied in the leading-edge region, and of favorable pressure gradients, attained by profile shaping.

Surface suction stabilizes the boundary layer via two mechanisms. The primary effect is to alter the mean velocity distribution to produce a more stable, fuller velocity profile, and a weaker, secondary effect is to decrease the overall boundary-layer displacement thickness, thereby reducing the associated Reynolds number Re_{δ^*}. Note that surface suction and profile shaping effects are both very sensitive mechanisms and that even weak suction or small pressure gradients have a strong influence on the stability characteristics of the boundary layer. According to White,[2] the most stable laminar boundary layer may be produced by applying "ideal" suction through a continuously porous surface. Idealized suction is, of course, no more than a concept; the ideal surface does not exist. Apart from aerodynamic considerations, realization of surface suction is determined by manufacturing capabilities, by structural criteria, and by operating conditions. Numerous designs have been assessed and rejected. Current HLFC design philosophy is to apply discrete localized suction through numerous laser-drilled, through-surface perforations. These perforations are typically 50 μm in diameter and are arranged in a staggered configuration with a pitch-to-diameter ratio of about 10. With this widely spaced configuration, it is generally assumed that each perforation behaves as if it were isolated, that is, that all aerodynamic interaction effects between perforations may be regarded as negligible.[3]

Although the application of discrete surface suction through microperforations can stabilize the boundary layer and delay the onset of transition, it is a sensitive technique that requires careful application. Previous workers have performed both experimental and computational investigations to determine the effect of discrete suction on a laminar boundary layer and to establish design criteria for LFC suction surfaces. The majority of fundamental research to date has focused on experimental studies to determine the global effects (boundary-layer stability, transition location, and integral parameters) for a particular suction configuration. Despite having a favorable effect on the stability of the boundary layer with low levels of suction, an upper limit exists beyond which an increase in the suction speed destabilizes the flow and causes the boundary layer to prematurely transition.[4–7] Experimental studies have been performed to determine the critical suction values for isolated and multiple-perforation arrangements.[8,9] However, the mechanisms by which discrete surface suction causes the boundary layer to transition are not fully understood.

Even though discrete suction is capable of delaying boundary-layer transition under certain circumstances, the physical details of how, and to what extent, concentrated suction perturbs and changes the local, and downstream, flowfield are unknown. At the most fundamental level, the flowfield induced by an array of LFC suction perforations may be expected to be of a three-dimensional nature, very likely strongly so, and considerably different from the idealized situation of continuously distributed suction.[5,10–12] Moreover, one may anticipate the presence of a variety of complex physical phenomena, for instance, trailing longitudinal vortices, nonuniformity of the mean flow, strong crossflow velocities, and local streamline curvature (Fig. 1). These conjectures are supported by computational studies performed by MacManus and Eaton,[13] MacManus et al.,[14] and MacManus[15] on isolated and multiple real-scale, i.e., actual flight dimensions, perforations, as well as on isolated superscale perforations.

It is important to establish whether such flowfield features arise for LFC perforations because any or all of these phenomena will influence the stability of the laminar boundary layer. Streamwise vorticity and spanwise modulations of the mean flow, for instance, are known to strongly affect the behavior of other disturbances that can destabilize the boundary layer.[5,16–18] The successful design and application of LFC requires knowledge of the circumstances under which flow phenomena induced by discrete suction arise and of the extent and characteristics of these flow phenomena. Some previous workers have investigated the detailed flowfields induced by superscale perforations using rudimentary flow visualization techniques.[10,12,19] Although these experiments are noteworthy, no quantitative flowfield measurements were made, and the suction configurations were predominantly for closely spaced rows of perforations ($s/d \approx 5$).

The objective of the present work is to acquire fundamental insights into the flow physics of LFC suction surfaces by performing a unique series of high-resolution, three-dimensional, laser Doppler velocimetry (LDV) flowfield measurements. The flow features induced in a laminar boundary layer by discrete surface suction are determined and analyzed with respect to LFC suction surface design. Critical suction limits and aerodynamic design criteria are established, and the transition mechanism is revealed. In addition, the detailed flowfield measurements provide high-quality data for validation of a technique for predicting the aerodynamic characteristics of generic suction surface configurations.[14,15,20]

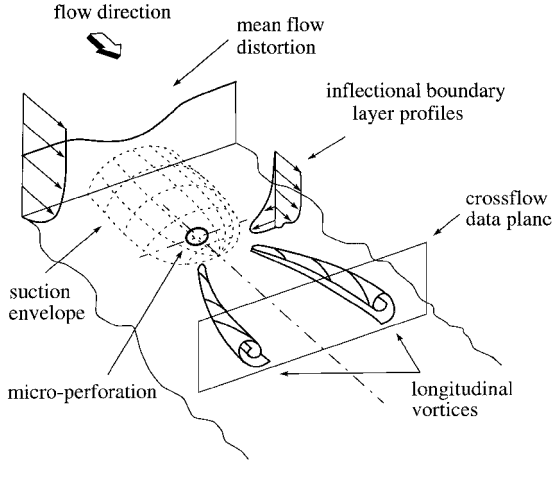

Fig. 1 Schematic of the flowfield induced by an isolated HLFC suction perforation.

II. Experiment Design

Because of the prohibitively microscopic scale, in the order of tens of microns, of an actual LFC suction perforation, no detailed velocity data have yet been produced for the flowfield under flight conditions. The only currently feasible solution[15] is to scale up the perforation size so that the detailed flowfield may be mapped, nonintrusively, using a high-resolution LDV measurement system.

To ensure that the flowfield induced by a superscale perforation exhibits the same features as those of an actual HLFC suction perforation, dynamic similarity must be preserved. Neglecting pressure gradient effects, a dimensional analysis reveals that the appropriate dimensionless groups include d/δ^*, V_h/U_e, Reynolds number based on displacement thickness Re_{δ^*}, L/d, suction Reynolds number Re_d, unit Reynolds number Re', and freestream Mach number M_∞. At cruise conditions, typical LFC values for these parameters are $d/\delta^* \approx 0.75$, $V_h/U_e \approx 0.20$, $Re_{\delta^*} \approx 900$, $L/d \approx 17$, $Re_d \approx 100$, $Re' \approx 6 \times 10^6$, and $M_\infty \approx 0.80$.

A group of superscale (of order 20:1) experiments were designed in which the parameters d/δ^*, V_h/U_e, Re_{δ^*}, L/d, and Re_d were preserved. This gives a perforation diameter that is still very small ($d \approx 1$ mm). For such microscale flowfield measurements of a sensitive laminar boundary layer, it is crucial that the technique used does not interfere with the flow. For this reason a high-resolution LDV was selected. Although the unit Reynolds number and Mach number of the experiment did not match those under flight conditions and the influence of an array of perforations was neglected, it was anticipated that all of the primary effects of applying discrete suction through microperforations were captured. To isolate the effects of discrete suction on a laminar boundary layer, a zero pressure gradient was set. Computational investigations reveal that compressibility does not have a significant effect on the primary flowfield characteristics.[15] Nevertheless, as compressibility has a stabilizing influence on the laminar boundary layer, it is expected that the critical suction parameter $G_{k\,\mathrm{crit}}$ would increase.

The flowfields induced by isolated, superscale perforations were examined for both sub- and supercritical suction configurations (V_h/U_e varied from 0.15 to 2.0). For an isolated perforation, one of the most important parameters is d/δ^*; preservation of this parameter was, therefore, prioritized when designing these experiments. Three perforation diameters were selected ($d = 0.8$, 1.0, and 1.3 mm) to provide a range of d/δ^* between 0.68 and 1.05, and the freestream velocity ranged between 12.2 and 16.2 m/s.

III. Experimental Apparatus

A. Wind-Tunnel Model and Suction System

The experiments were performed in a low-speed, low-turbulence wind tunnel at Bristol University. The working section is 0.8 × 0.6 m, and the freestream turbulence level is less than 0.1% at the operating speeds. The model was a purpose-built aluminum flat plate, 1450 mm long × 795 mm wide × 25.4 mm thick, with an elliptical leading edge (5.8:1) and an adjustable trailing-edge flap. The model was mounted horizontally along the working section centerline, and the surface was carefully hand polished to reduce surface roughness. The three suction perforations were located on the upper surface 450 mm from the leading edge and were spaced 80 and 100 mm apart in the spanwise direction. A connector was attached to each perforation to provide a constant hole cross-sectional area and a total perforation depth of 16.4 mm in each case; thus, the L/d ratio ranged between 12.6 and 20.5. Static pressure tappings (0.5-mm bore) were positioned on the upper surface, 12 on each side, 80 mm from the plate edge. The trailing-edge flap was adjusted to provide a stable boundary layer, and the static pressure along the plate was

measured using an inclined manometer. The plate and flap were adjusted until the static streamwise pressure gradient was nominally zero and symmetric about the streamwise axis.

Transition was monitored using a miniature (1.3-mm-diam) flush-mounted, hot-film sensor element (TSI Model 1268) in conjunction with a constant-temperature anemometer (TSI Model 1054B) and an oscilloscope. This probe was mounted on a detachable insert, which enabled it to be positioned 180 mm directly downstream of each suction perforation.[15]

The perforations were connected, one at a time, to the suction system, and the flow rate was set and controlled using an electronic mass flow controller (Omega FMA 1416). Both hot-wire anemometer and LDV measurements independently verified that the flow at the perforation inlet was steady, as desired, and that no perturbations from the suction system reached the surface.

B. LDV System

Nonintrusive velocity measurements were performed using the three-component LDV system at Bristol University. This system consists of a 5-W argon-ion laser, a transmitter box, two fiber-linked optic heads, a three-axis traverse mechanism, and three burst spectrum analysers. The system is operated in the off-axis mode, which reduces the measurement volume to a spheroid of approximately 80-μm diam for a focal length of 600 mm. This measurement volume size is based on the transit distance (transit time $\times$ velocity). The six beams are carefully aligned using a pinhole meter procedure,[21] which enables measurements to be obtained down to approximately 50 μm from the surface. The three-axis traverse mechanism provides a spatial precision of 5 μm in all three directions.

IV. Measurements and Observations

A. Introduction

The objective of these experiments is to acquire a detailed description of how an LFC suction perforation affects a laminar boundary layer. To provide a datum set of measurements (with no suction applied), the characteristics of the unperturbed boundary layer were examined by acquiring the three-dimensional velocity profiles and the "natural" transition Reynolds number. Detailed investigations of the perforation flowfield, with suction applied, were then made by measuring the three velocity components on planes normal to the freestream direction, both upstream and downstream of the perforation. Three-dimensional boundary-layer velocity profiles were also taken at locations downstream of the perforation. These were obtained along centerline positions as well as at off-center locations coincident with one of the longitudinal vortex cores, which were found to occur aft of the perforation. The critical suction speed for each perforation, over a range of freestream speeds, was also determined. To monitor the boundary-layer state and transition process over an extended surface area, the rms velocity was measured on planes parallel to the plate surface. These configurations included cases with subcritical and critical suction speed.

B. "Natural" and Suction-Induced Transition

The critical Reynolds number for "natural" transition was measured using the surface-mounted hot-film probe, which was positioned at three spanwise locations, each 630 mm from the leading edge. The freestream speed was gradually increased, and the boundary-layer state was monitored using the oscilloscope. For ease of identification, transition was deemed to occur at the first intermittent signal, and the transition Reynolds number was found to be in the range from 1.53×10^6 to 1.6×10^6.

Although the application of suction through microperforations can stabilize the boundary layer, there exists a limit beyond which an increase in the suction speed will destabilize the flow and cause transition.[4,5,9,12] For LFC design purposes it is important to determine what these critical suction limits are. To this end gradually increasing suction was applied, and the state of the boundary layer was determined using the flush-mounted hot-film sensor. Output from the sensor revealed that the transition process commenced with the growth of Tollmien–Schlichting waves, which was followed by increasing levels of intermittency and finally by a fully turbulent flow. The transition process was monitored over a range of freestream velocities between 12.2 and 28.4 m/s.

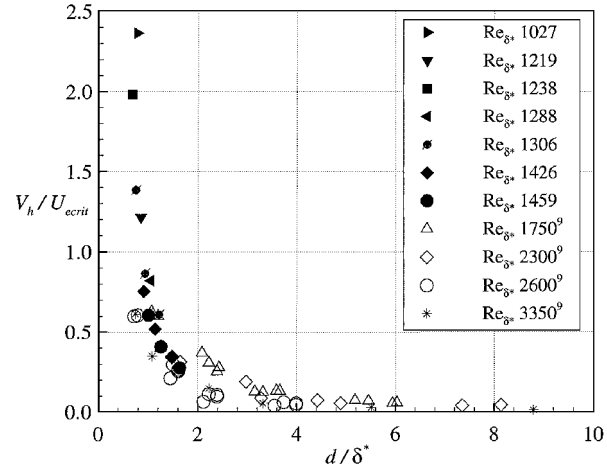

Fig. 2 Comparison of measured critical suction velocity with previously reported transonic results.[9]

Similar to the "natural" transition process just described, the critical suction speed ratio is determined by gradually increasing V_h/U_e until the first intermittent signal is detected using the hot-film sensor. The observed critical suction speed ratio $V_h/U_{e\,\mathrm{crit}}$ is plotted against d/δ^* in Fig. 2. As can be seen, the results are grouped very well together, and the critical suction speed ratio is shown to increase as d/δ^* is decreased. Good agreement is also found when compared to previous transonic measurements.[9] This plot also appears to indicate that, as d/δ^* is decreased, there may be a limit below which suction does not precipitate transition ($d/\delta^* < 0.6$). There is much uncertainty concerning the maximum allowable suction rate for LFC perforated surfaces. To avoid premature tripping of the laminar boundary layer, current LFC design philosophy employs an upper limit of approximately 50 m/s on the suction speed V_h, at cruise conditions.[22] From Fig. 2, and ignoring compressibility effects, this restriction may be too severe for the leading-edge region of a typical LFC configuration ($d \approx 50\,\mu$m, $d/\delta^* \approx 1.0$, and $M_\infty \approx 0.80$). Note that due to the observed transition mechanism (see Sec. IV.C), the location of the hot-film sensor may indicate a slightly optimistic critical suction speed ratio. Based on two sets of measurements, which monitored the variation of the rms velocity with both the suction speed ratio and the streamwise location, it is calculated that the measured critical suction speed ratios may be overestimated by about 10%.

These experiments show that suction does not induce an abrupt transition from a laminar to a turbulent boundary layer. Rather, there is a range of suction speed ratios over which the first occurrences of intermittency gradually develop into a fully turbulent flow. From the measurements it is evident that the band of suction velocities over which the boundary layer becomes fully turbulent depends on d/δ^*. In particular, as d/δ^* increases, the evolution from initial disturbances to a fully turbulent signal occurs over a much smaller suction range. For a typical d/δ^* value of approximately 1.0, the transition process commences when $V_h/U_e \approx 0.6$, and the suction speed ratio must be increased to about 0.8 before a fully turbulent signal is observed.

C. Suction Perforation Flowfield Measurements

The flowfield was mapped by measuring the three-component mean velocities in the vicinity of the perforation. These measurements were taken at discrete locations on planes normal to the flow stream direction, $1d$ upstream and $1d$, $3d$, $5d$, and $8d$ downstream of the perforation. In each plane (typically 8×3 mm) about 550 data points were acquired. The three-dimensional boundary-layer profiles were measured at locations up to $123d$ downstream. These mean velocity profiles were recorded both along the perforation centerline and also at off-center positions, which enable the trailing longitudinal vortices to be studied.

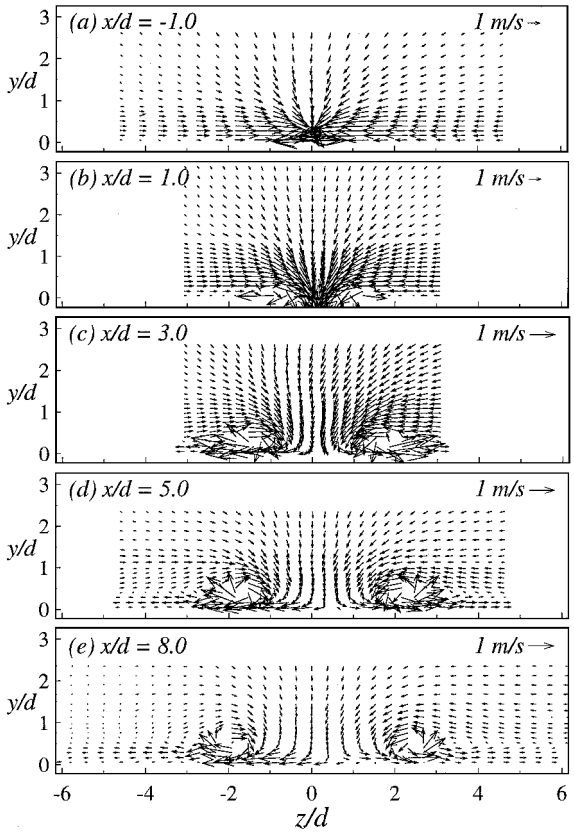

Fig. 3 Sequence of $V-W$ velocity vectors in crossflow data planes upstream and downstream of a 1.3-mm hole with subcritical suction with $d = 1.3$ mm, $d/\delta^* = 1.05$, $V_h/U_e = 0.58$, and $Re_{\delta^*} = 1290$. Note that vector scale used in panels a and b differs from that used in panels c, d, and e.

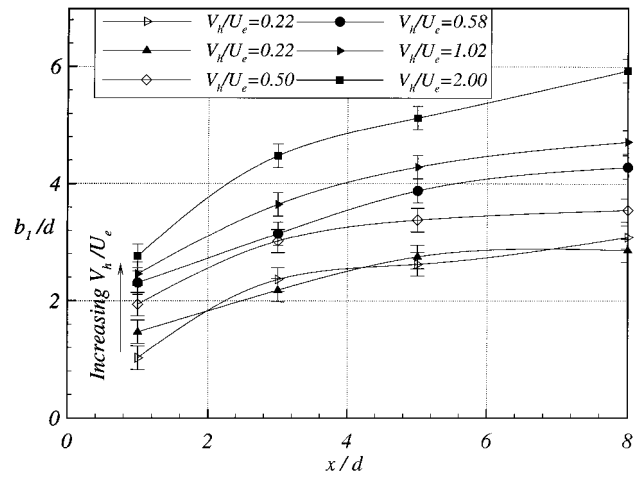

Fig. 4 Spanwise spacing of suction-induced longitudinal vortices as a function of streamwise position, x/d.

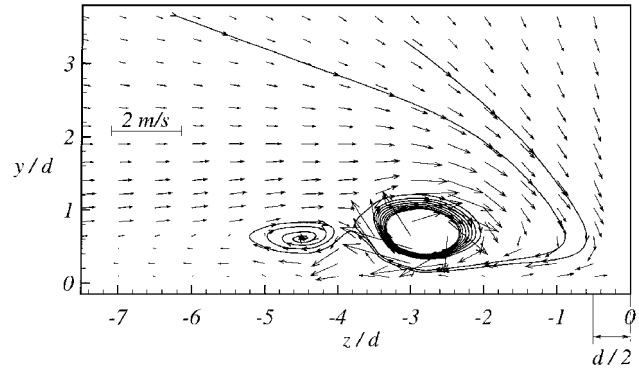

Fig. 5 Corotating vortices highlighted using two-dimensional streamtraces in y–z crossflow data plane $8d$ downstream of hole: $d = 0.8$ mm, $d/\delta^* = 0.68$, $V_h/U_e = 2.0$, and $Re_{\delta^*} = 1240$.

Measurements were taken in normal planes downstream of the perforations with no suction applied. It was found that the presence of the perforations has no discernible effect on the mean velocity profiles of the boundary layer, as reflected in the observed uniformity of the mean streamwise, crossflow, and wall-normal velocity distributions.

Longitudinal Counter-Rotating Vortices

Saric[11] proposes an analogy between the flow over a suction perforation and the flow over a finite wing, where a pair of wing tip vortices are generated. As anticipated,[12,13,19] when suction is applied the most prominent feature to develop is a pair of counter-rotating longitudinal vortices that occurs aft of each perforation. This vortex pair appears regardless of whether subcritical or supercritical suction is applied. However, the strength and the definition of the vortex pair both increase as the suction speed is increased. A typical evolution of the longitudinal vortices is shown in Fig. 3, where the $V-W$ velocity vectors are plotted in a sequence of crossflow data planes from $1d$ upstream to $8d$ downstream of a 1.3-mm perforation with subcritical suction applied ($d/\delta^* = 0.77$ and $V_h/U_e = 0.58$). The vortex cores decay and expand as they progress downstream.

As the pair of longitudinal vortices is convected downstream, the spanwise, or lateral, spacing of the pair increases and the vortex center, which is hereafter referred to as the core, moves away from the wall. Immediately aft of the perforation, the spanwise spacing of the cores increases appreciably, but farther downstream the vortices become more closely aligned with the freestream direction.

The lateral spacing of the longitudinal vortices was determined at a distance $1d$, $3d$, $5d$, and $8d$ downstream of the perforation center. The position of each vortex core was estimated from the mean velocity and streamwise vorticity plots. As already noted, the lateral spacing increases as the longitudinal vortices are convected downstream. The lateral spacing also expands with strengthening suction speed. This is shown in Fig. 4, where, for a range of perforation diameters and suction velocities, the dimensionless vortex spacing b_1/d is plotted as a function of dimensionless streamwise position x/d. Even at $8d$ downstream, where the vortex core typically lies about $0.50d$ from the plate surface, the lateral spacing of the vortex pair is still growing.

Multiple Longitudinal Vortices

When high, though not necessarily critical, suction velocities are applied ($V_h/U_e = 0.58$, 1.02, and 2.00), there is a marked difference in the vortices that are generated downstream of the perforation. Instead of a single pair of counter-rotating longitudinal vortices, four vortices appear downstream of the perforation: a pair of corotating vortices on each side of the centerline. The appearance of these secondary vortices outboard of the primary pair has also been previously observed by Meyer[19] using smoke visualization techniques. Meyer noted that, after the development of the first pair of vortices, an increase in the suction speed results in the generation of auxiliary pairs of vortices (although he observed them only at very low freestream speeds and made no comment on their sense of rotation). During the present investigation, these secondary, corotating vortices were observed for both sub- and supercritical suction velocities. They are located abeam of the primary vortices but are markedly weaker. The corotating vortices are still evident $8d$ downstream of the perforation and are highlighted using two-dimensional streamtraces in Fig. 5.

When high suction is applied, the appearance of secondary vortices abeam of the primary longitudinal vortices is not surprising. What is noteworthy, however, is that these vortices have the same sense of rotation as the primary vortex. Because of the locally large crossflow velocities induced by the suction perforation, the occurrence of these corotating vortices may also be analogous to the formation of similar vortex structures in crossflow-dominated flows.

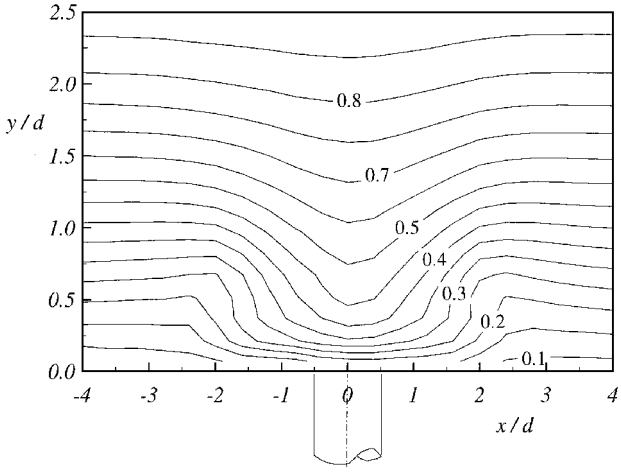

Fig. 6 Facing upstream, contours of streamwise velocity, U/U_e, on a normal plane 8d downstream with subcritical suction applied: d = 1.0 mm, d/δ^* = 0.77, V_h/U_e = 0.50, and Re_{δ^*} = 1030.

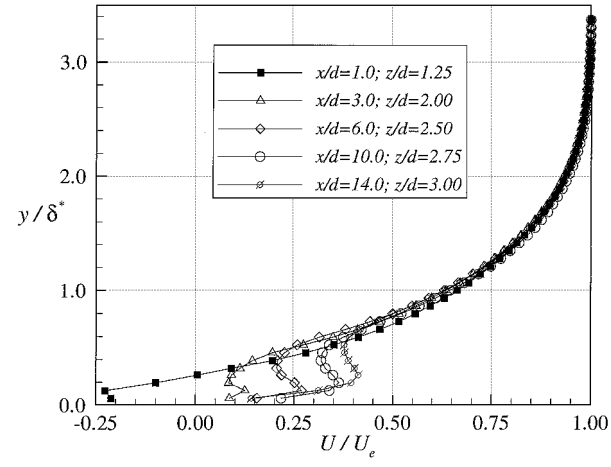

Fig. 7 Streamwise velocity profiles measured along a longitudinal centerline with supercritical suction applied: d/δ^* = 0.68, V_h/U_e = 2.0, and Re_{δ^*} = 1240.

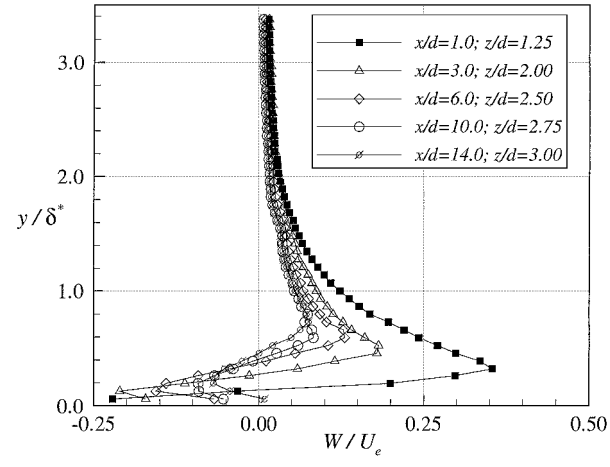

Fig. 8 Lateral velocity profiles measured along a longitudinal vortex centerline with supercritical suction applied: d/δ^* = 0.68, V_h/U_e = 2.0, and Re_{δ^*} = 1240.

Effect of Discrete Suction on Streamwise Velocity Component

Wall suction stabilizes the flow via two mechanisms: It decreases the boundary-layer thickness, thereby reducing Reynolds number based on displacement thickness Re_{δ^*}, and it improves the stability characteristics of the streamwise velocity profile. The thinning of the boundary layer and the associated decrease in the curvature term $\partial^2 U/\partial y^2$ are borne out by the deflection of the measured U velocity contours both upstream and downstream of the perforation. Downstream of the perforation, the spanwise extent of this effect is bounded by the spacing of the vortices. Figure 6 clearly shows that, due to the three-dimensionality of the suction perturbation, there are large spanwise variations in the mean flow, even at 8d downstream of the perforation center. For a HLFC suction surface, with an array of discrete perforations, these suction-induced, local nonuniformities of the mean flow may produce a surface roughness effect, thereby increasing the susceptibility of the boundary layer to external disturbances.

Three-Dimensional Boundary-Layer Profiles

To further investigate how the boundary layer is affected, detailed three-dimensional velocity profiles were measured at locations both along the perforation centerline and at x–z stations corresponding to a surface-projected locus of one of the vortex cores. Suction has a strong effect on the streamwise velocity profiles downstream of the perforation. Relative to the unperturbed reference profile, the local suction boundary layer exhibits a fuller streamwise velocity profile with large velocity gradients in evidence closest to the wall. [At 5d downstream of the suction perforation, $(\partial U/\partial y)|_w$ is approximately an order of magnitude greater than the undisturbed value.]

Streamwise and lateral velocity profiles at stations along the cores of the longitudinal vortices are presented in Figs. 7 and 8, respectively. This example is for a supercritical suction speed. The retardation of the streamwise velocity at the vortex center produces inflectional velocity profiles; indeed, the flow is observed to be completely reversed in the station immediately downstream ($x/d = 1.0$) of the perforation. The lateral velocity profiles also exhibit a point of inflection and, as already mentioned, this type of velocity profile is inherently unstable. The peak level of measured crossflow velocity is approximately $1.0U_e$, which is at least one order of magnitude greater than the crossflow velocities associated with typical crossflow vortices over a swept wing ($W_{\max} \approx 0.05U_e$). Also evident in the streamwise and lateral velocity profiles is the evolution of the longitudinal vortex as it progresses downstream. The vortices expand and decay as they are convected downstream and as the cores migrate away from the surface.

RMS Velocity Scans in Horizontal Planes

To monitor the boundary-layer state over an extended area, the rms velocity was measured on planes parallel to the surface. These horizontal scans were taken using the LDV in single-component mode, and the measured mean velocity component was in an approximately streamwise direction. The purpose of this procedure was to utilize the rms velocity as an indicator of disturbance level and distribution. As with all LDV systems, the measured rms velocity is prone to being artificially high; this is due to the finite size of the measuring volume and to electrical noise. Moreover, this effect is more pronounced in areas of high-velocity gradients, such as close to a surface.[23] The recorded rms value is also highly dependent on the bandwidth setting of the signal processor. In spite of these limitations, and with careful use, this approach provides useful results. The horizontal scans were taken at heights of 0.1, 0.4, and 0.5 mm, and the bandwidth setting in the signal processor was kept constant throughout. The surveyed area extended from 5.0 mm upstream to 160.0 mm downstream of the perforation centers. Two typical scans, taken at 0.1 and 0.5 mm from the surface, for a supercritical suction speed, are presented in Fig. 9. Downstream of $x/d \approx 10$, the scan planes lie below the vortex cores, and the flow is considered to be turbulent when the rms velocity is greater than approximately 1.0 m/s.

For this case, in each scan the development of two turbulent regions (beginning at about $x/d = 75$), positioned symmetrically about the centerline, can be clearly seen. These regions are where the trailing longitudinal vortices become unstable and precipitate transition. The total included angle of the pair of turbulent regions at both heights is about 15 deg. In Fig. 9a the scan is very close to the wall, and the turbulence level increases rapidly with streamwise distance. The scan in Fig. 9b lies about halfway between the vortex core and the wall. Within each turbulent region the vortex core is bordered by distinct ridges of peak turbulence. Based on

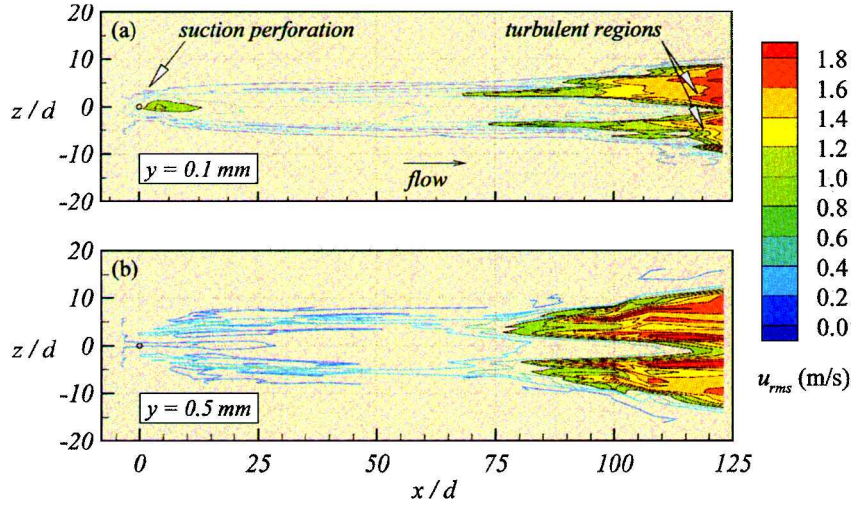

Fig. 9 Horizontal scans of (approximately streamwise) rms velocity component fluctuations, taken close to the surface. A pair of turbulent regions shows the laminar–turbulent transition of the trailing vortices, which form downstream of the suction hole with d = 1.3 mm, d/δ^* = 1.05, V_h/U_e = 1.02, and Re_{δ^*} = 1290. Distance from wall: a) 0.1 mm and b) 0.5 mm.

these two images it appears that the instabilities are initiated on a slender conical surface that surrounds each vortex core. These disturbances grow and merge until a fully turbulent wedge is formed. In conclusion, the suction-induced transition process is initiated by instabilities in the streamwise vortices, which ultimately transition and merge to form a turbulent wedge.

Because of the off-center, symmetric location of the turbulent regions, the initial signs of transition may pass undetected on each side of the hot-film sensor (which was positioned on the centerline), and, hence, the critical suction velocities presented in Sec. IV.B may be slightly overestimated.

V. Measurement Uncertainties

Many interdependent factors affect LDV measurements, and it is difficult to quantify the overall measurement accuracy. Where possible, however, the sources of uncertainty due to the model geometry, suction system, and LDV were identified and analyzed, and their influence on the overall data fidelity was assessed.[15] Uncertainties associated with the LDV system include positional accuracy, gradient bias, velocity bias, statistical errors due to finite sample size, optical uncertainties, alignment uncertainties, calibration and transformation uncertainties, particle behavior, and frequency measurement. A comprehensive and full analysis of these possible uncertainty sources, and of their influence on the measurements, is presented by MacManus[15] and MacManus et al.[24]

The interdependent nature of the various sources of uncertainty, both systematic and random, makes any estimate of the overall error difficult to ascertain. Simply to quote a maximum error for the measurements, such as occurs at the vortex cores where the positional error is substantial (~1%), would be quite misrepresentative of the majority of the flowfield. Therefore, the estimated major uncertainties, at two characteristic positions ("best" case and "worst" case) within the flowfield, are determined. By simply summing the individual uncertainty components, it could be concluded that the peak overall uncertainties are of the order of 0.5% in the freestream and less than 2% in the vortical regions.

VI. Analysis of Results

The measurements clearly show that the flowfield induced in a laminar boundary layer by an LFC suction perforation is highly three dimensional and profoundly different from the idealized concept of continuously distributed suction. The field measurements and observations presented illustrate and quantify, for the first time, the rich variety of flow features that occur. This adds considerably to the knowledge and understanding of the flow physics of how concentrated suction perturbs and changes the local flowfield of an LFC suction surface. Although the main concern of this work was a fundamental experimental investigation of the flowfields induced by LFC suction perforations, some valuable engineering conclusions and design criteria can also be drawn from these measurements. We now present further analyses, the first to establish a new critical suction parameter, and the second to assess the possibility of interaction between the suction-induced longitudinal vortices and the crossflow vortices embedded in the boundary layer of a swept wing.

A. Critical Suction Predictions

There is much uncertainty concerning the maximum allowable suction rate for LFC perforated surfaces.[9,10,22] For LFC design purposes, and to avoid premature tripping of the laminar boundary layer, it is essential that a critical suction criterion be established. A variety of methods have been proposed, including a critical perforation Reynolds number $Re_{d\,\mathrm{crit}}$ (Refs. 11 and 25) and an equivalent roughness analogy.[8,9,17] Although it is still employed in current LFC design practice,[25] the simple critical Reynolds number has been shown to be oversimplistic and too restrictive a parameter.[15] A more sophisticated method is required to relate the level of suction-induced disturbance to the local boundary-layer stability characteristics. Previous workers[8,9,17] have drawn parallels between the flowfield downstream of a suction perforation and that of a three-dimensional roughness element, for which many data are available. The primary features exhibited by both flowfields are longitudinal vortices. It has been mooted that the strength of the suction-induced vortices and the size of the sucked streamtube envelope (see Fig. 1) increase with perforation suction in a manner similar to that in which the strength of the roughness-induced vortices increases with element height. Based on these comparisons between the imagined shape of the sucked streamtube and the roughness element geometry, a variety of equivalent roughness analogies has been offered as an engineering tool to predict the critical suction limits. Blanchard et al.[8] proposed the parameter $P_k = (y_k/\delta^*)\sqrt{Re_{\delta^*}}$ to predict the critical suction speed ratio. This assumes a rectangular cross-sectional shape for the sucked streamtube and then uses the mass flow $\dot{m}$ to calculate the streamtube height y_k.

To determine the actual shape and dimensions of the sucked streamtubes, the current flowfield measurements were analyzed by interpolating the three-component measurements onto a computational domain encompassing the suction perforation region. The interpolation was performed using an inverse distance algorithm,[26] and the streamline deflections around the suction perforations were calculated from the interpolated field velocities. Using these experimental results, we have shown previously[15] that Reneaux's roughness analogy[27] is unrealistic and inadequate for predicting the critical suction limits.

B. New Critical Suction Parameter

The sucked streamtube is the locus within which all of the fluid is ingested by the suction perforation, and a schematic of this suction envelope for an isolated perforation, as anticipated by Goldsmith,[10]

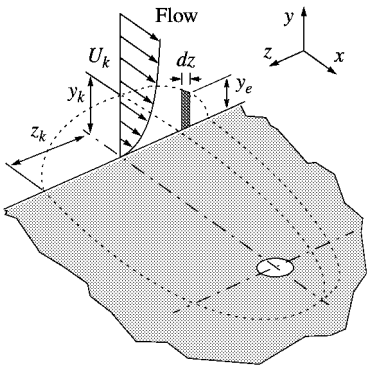

Fig. 10 Schematic of a typical sucked streamtube of an isolated perforation as anticipated by Goldsmith.[10]

is shown in Fig. 10. To establish a practical design criterion for LFC critical suction limits, the approach of Goldsmith[10] is adopted here to relate known quantities to a streamtube Reynolds number $Re_k = U_k y_k/\nu$. This Reynolds number is based on the characteristics of the sucked streamtube, as shown in Fig. 10, and it is expected that the streamtube Reynolds number Re_k is a measure of the disturbance introduced into the laminar boundary layer. Analogous to the situation with roughness elements, it is anticipated that a single critical Reynolds number exists. For LFC design purposes, however, the streamtube Reynolds number Re_k is unknown, and it is logical to relate it to a parameter whose constituent variables are known or may be estimated. Therefore, following Goldsmith, a new parameter G_k is investigated here as a potential critical suction indicator.

It is assumed that within the region of the suction envelope the velocity gradient is constant:

$$\frac{\partial U}{\partial y} = \left.\frac{\partial U}{\partial y}\right|_w \tag{1}$$

then using the notation described in Fig. 10

$$Q_h = 2\int_0^{z_k}\int_0^{y_e} y\frac{\partial U}{\partial y}\,\mathrm{d}y\,\mathrm{d}z \tag{2}$$

which yields[15]

$$Q_h = \frac{y_k^3}{2}\frac{\partial U}{\partial y}I_1 \tag{3a}$$

where

$$I_1 = 2\int_0^{z_k/y_k}\left(\frac{y_e}{y_k}\right)^2 \mathrm{d}\frac{z}{y_k} \tag{3b}$$

thus

$$y_k^2 = \left(Q_h \Big/ I_1\frac{\partial U}{\partial y}\right)^{\frac{2}{3}} \tag{4}$$

From the initial assumption of constant velocity gradient normal to the wall

$$\frac{U_k y_k}{\nu} = \frac{y_k^2}{\nu}\frac{\partial U}{\partial y} \tag{5}$$

therefore, from Eq. (4),

$$\frac{U_k y_k}{\nu} = \frac{1}{\nu}\left(\frac{2}{I_1}\right)^{\frac{2}{3}} Q_h^{\frac{2}{3}}\left(\frac{\partial U}{\partial y}\right)^{\frac{1}{3}} \tag{6}$$

In Eq. (6), although I_1 is unknown, by assuming that $I_1 = f\{Re_k\}$, then the following applies:

$$Re_k = \frac{U_k y_k}{\nu} = f\left\{\frac{1}{\nu}Q_h^{\frac{2}{3}}\left(\frac{\partial U}{\partial y}\right)^{\frac{1}{3}}\right\} = f\{G_k\} \tag{7}$$

For the experimentally investigated cases, a linear relationship is found (over both sub- and supercritical suction configurations) between the measured streamtube Reynolds number Re_k and Goldsmith's[10] parameter $[(1/\nu)Q_h^{2/3}(\partial U/\partial y)^{1/3}]$. The variables used to define G_k (Q_h, ν, and $\partial U/\partial y$) are known, and from this simple relationship the critical suction parameter $G_{k\,\mathrm{crit}}$ is estimated

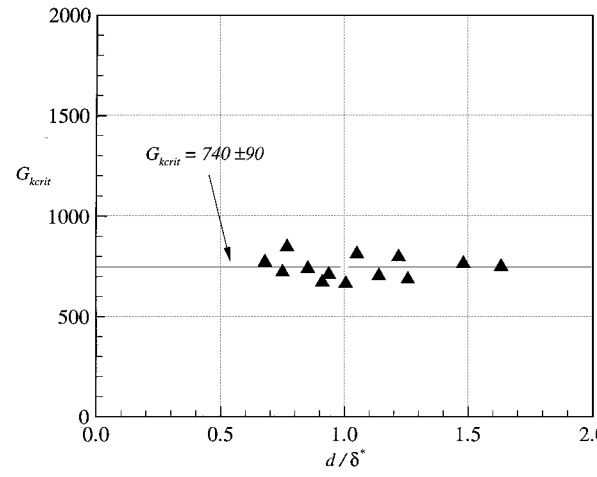

Fig. 11 Variation of predicted critical suction parameter $G_{k\,\mathrm{crit}}$ with d/δ^*.

for the observed critical suction configurations (see Sec. IV.B). In Fig. 11, the calculated $G_{k\,\mathrm{crit}}$ is plotted against d/δ^*, and the data are found to concentrate around a constant value of $G_{k\,\mathrm{crit}} \approx 740 \pm 90$. This result indicates that G_k is a parameter that uniquely quantifies the effect of suction through a perforation on the boundary-layer stability.

These experimental results reveal that a simple engineering design criterion may be established for critical suction limits. Although Fig. 11 shows that a unique $G_{k\,\mathrm{crit}}$ of approximately 740 ± 90 applies for an isolated perforation under low-speed conditions, it is to be expected that this criterion will need to be adjusted for flight conditions. Previous workers have shown that the critical criterion ($P_{k\,\mathrm{crit}}$) for an array of suction perforations can be obtained by offsetting the results obtained for an isolated perforation by a constant value.[8,9] Similarly, it is possible that the $G_{k\,\mathrm{crit}}$ for an array of microperforations could be extrapolated from the results obtained here for a single perforation, though further experimental evidence is needed to substantiate this conjecture.

C. Spanwise Spacing of Longitudinal Vortices

In the primary HLFC application, i.e., wings with sweep, the flow is three dimensional, and crossflow instabilities are, therefore, expected to play a significant role when considering the stability of the boundary layer.[28] Crossflow instability is characterized by stationary, corotating vortices that are aligned in the freestream direction and have a typical wavelength of approximately four times the boundary-layer thickness.[28] When suction is applied through discrete perforations, there is a possibility of interaction between these crossflow vortices and the longitudinal vortices that are generated downstream of an active suction perforation. Hence, the spanwise spacing of the longitudinal vortices that are created by a suction perforation may be an important parameter.[11] Although the wind-tunnel model in this experiment is a flat plate with a zero nominal pressure gradient, it is expected that the primary spacing characteristics of the longitudinal vortices have been captured.

In wind-tunnel experiments on a swept wing, Radeztsky et al.[29] has shown that the stability of stationary crossflow vortices, which dominate the three-dimensional transition process in low-disturbance environments, is strongly affected by small, isolated roughness elements located at the attachment line. They showed that the disturbance amplification factors are increased, and the flow destabilized, by the injection of streamwise vorticity on the scale of the stationary crossflow vortices. The possibility of the streamwise vorticity introduced into the boundary layer by HLFC suction perforations having a similar effect on crossflow vortices is now considered.

There are two lateral length scale parameters associated with the streamwise vorticity introduced by a suction perforation: the spanwise spacing b_1 of a local pair of counter-rotating vortices downstream of an individual perforation and the spanwise spacing b_2 of the vortices downstream of adjacent perforations. Similar to the

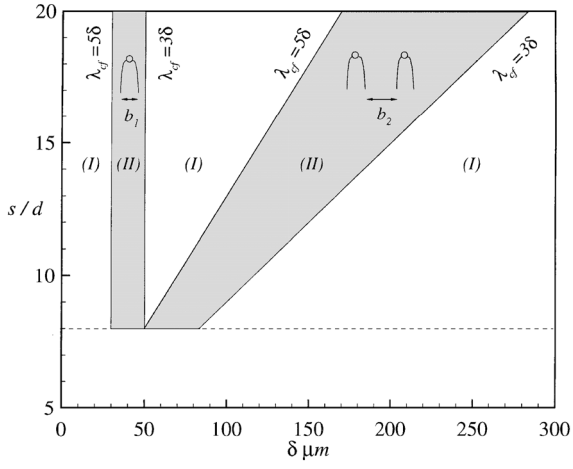

Fig. 12 Map of HLFC suction surface configurations, where the spanwise spacing of suction-induced and crossflow vortices coincide: I, interactions unlikely, and II, interactions likely.

formation of crossflow vortices, it is possible that in the presence of a three-dimensional mean flow these counter-rotating vortices may generate a corotating vortex structure. By assuming a perforation local vortex spacing of $b_1/d = 3$ (Fig. 4), a perforation diameter of 50 μm and a crossflow vortex spacing λ_{cf} between 3δ and 5δ, the configurations where the vortex spacings (crossflow and suction-induced) coincide are presented in Fig. 12. The shaded regions show the combinations of s/d and δ that may be susceptible to aerodynamic interactions between the suction-induced vortices and crossflow vortices and are, therefore, to be avoided in design. This plot shows that, unless the boundary layer is very thin ($\delta \approx 50$ μm), the vortices spaced between adjacent perforations ($\lambda_{cf} \approx b_2$) are the most likely source of vorticity for a disturbance interaction on the scale of the crossflow vortices. For instance, in the leading-edge region of a typical HLFC wing under transonic cruise conditions, where the boundary-layer thickness is of the order of 200 μm, the spanwise spacing of the suction-induced and crossflow vortices coincide when the perforation spacing s/d is increased above 15. Indeed, some present-day HLFC suction surfaces use an s/d of up to 15 to create a larger pressure drop across the surface for a given average suction coefficient. Therefore, when designing a suction surface, it is important to take into account the possibility of detrimental vortex interaction occurring.

VII. Summary and Conclusions

The detailed flowfield of an isolated LFC suction perforation was successfully investigated and mapped, and a rich variety of flow features and phenomena was identified. By utilizing three different superscale perforation diameters (in conjunction with the high spatial resolution attainable with an accurate LDV system), the important dimensionless parameters d/δ^*, V_h/U_e, Reynolds number based on displacement thickness Re_{δ^*}, L/d, and suction Reynolds number Re_d were preserved. For an extensive range of configurations, accurate, nonintrusive measurements were obtained using a three-component LDV system.

The velocity measurements confirm that the flowfield of an LFC suction perforation is of a highly three-dimensional nature. Flow features, which were observed and which depended on values of d/δ^* and V_h/U_e, included two counter-rotating longitudinal vortices, multiple longitudinal vortices, and inherently unstable boundary-layer velocity profiles.

The critical suction speed for isolated perforations, over a range of d/δ^*, was determined, and the critical suction limit was found to be inversely dependent on d/δ^*. As d/δ^* is reduced, there appears to be a limit ($d/\delta^* \approx 0.6$) below which suction through an isolated perforation will not provoke transition. Also, the current LFC design limit of approximately 50 m/s on the perforation average suction speed V_h may be too restrictive. Surveys of the rms velocity in planes parallel to the surface show that suction-induced transition is a gradual process (dependent on d/δ^*), which results in the development of two turbulent regions downstream of the suction perforation. This discovery indicates that suction-induced transition is precipitated through instabilities of the longitudinal vortices.

Previously proposed roughness analogies based on the assumption of a rectangular streamtube shape were evaluated and found to be misrepresentative and inadequate. A parameter first proposed by Goldsmith, G_k, was investigated, and a new simple design criterion for critical suction has been established ($G_{k\,\mathrm{crit}} = 740 \pm 90$).

For low and moderate suction, two counter-rotating longitudinal vortices were formed downstream of the perforation. When high, though not necessarily critical, suction velocities are applied, four longitudinal vortices are generated aft of the perforation, consisting of a pair of corotating vortices on each side of the perforation centerline. As these vortices are convected downstream, the spanwise spacing between the cores increases, and the cores move away from the surface and become more closely aligned with the freestream direction. The spanwise spacings of the longitudinal vortices were found to increase with the suction speed ratio V_h/U_e. This may be an important consideration when applying discrete suction on a swept wing, where there is a possibility of interaction between the boundary-layer embedded crossflow vortices and the longitudinal vortices that are generated downstream of HLFC perforations. In the leading-edge region of a typical HLFC wing [$\delta \approx \mathcal{O}(200\ \mu\mathrm{m})$], this type of interaction is most likely when the perforation spacing, s/d, is increased above 15.

Along the centerline downstream of the perforation, the effect of discrete suction is to reduce the displacement thickness Reynolds number Re_{δ^*} and to produce more stable velocity profiles. However, inherently unstable inflectional boundary-layer profiles are generated elsewhere in the flowfield. Along the curve described by the vortex centerline, all three velocity components exhibit inflectional profiles, and the streamwise velocity profiles contain severe gradients in the vortex core. Within the region close to the perforation, crossflow velocity profiles, whose magnitudes are dependent on the suction speed, are generated.

In summary, an approach and measurement technique have been established for investigating, in detail, the flowfield of LFC suction surfaces. As a first step, this technique was applied to provide high-quality velocity measurements of several isolated perforations. The measurements produced in this initial investigation have enabled the flow features of the LFC suction surface to be identified, have provided understanding of the suction-induced transition mechanism, and have established directly applicable results in the form of critical suction limits, a critical suction parameter, and a design guide on the possibility of detrimental vortex interactions. These high-quality field data also serve as the basis for the validation of a prediction technique for the analysis of LFC suction perforations.

Acknowledgments

This work was funded by Airbus Industrie, and the authors thank Joachim Szodruch, Robert Hinsinger, and Daniel Arnal (CERT/ONERA) for their support. We also thank Martin Lowson and Rod Barrett, who made available the facilities at the University of Bristol, and Chris Swales and Jerry Rickards for their assistance, advice, and commitment.

References

[1] Holmes, B., "NLF Design and Applications Considerations," *Applied Viscous Flow Control for Drag Reduction*, Univ. of Kansas, Lawrence, KS, 1987, Chap. 6.

[2] White, F. M., *Viscous Fluid Flow*, 2nd ed., McGraw–Hill, New York, 1991.

[3] Poll, D. I. A., Danks, M., and Humphries, B. E., "The Aerodynamic Performance of Laser Drilled Sheets," *Proceedings of First European Forum on Laminar Flow Technology* (Hamburg, Germany), DGLR-Bericht 92-06, Deutsche Gesellechaft für Luft- und Raumfahrt, Bonn, Germany, 1992, pp. 274–277.

[4] Saric, W., and Reed, H., "Effect of Suction and Weak Mass Injection on Boundary Layer Transition," *AIAA Journal*, Vol. 24, No. 3, 1986, pp. 383–389.

[5] Gregory, N., "Research on Suction Surfaces for Laminar Flow," *Boundary Layer and Flow Control*, Vol. 2, edited by G. V. Lachmann, Pergamon, Oxford, England, UK, 1961, pp. 924–960.

[6] Gregory, N., and Walker, W. S., "Experiments on the Use of Suction Through Perforated Strips for Maintaining Laminar Flow: Transition and

Drag Measurements," Aeronautical Research Council, Repts. and Memoranda 3083, London, June 1955.

[7]Butler, S. F. J., "Current Tests on Laminar Boundary Layer Control by Suction Through Perforations," Aeronautical Research Council, Repts. and Memoranda 3040, London, Aug. 1957.

[8]Blanchard, A., Seraudie, A., and Plazanet, M., "Limite de Déclenchement de la Transition par Aspiration à Travers des Trous Isolés sur un Profil Laminaire en Écoulement Transsonique," ONERA-Département d'Études et de Récherches en Aerothermodynamique, Rept. 38/5006.21, Toulouse, France, March 1990.

[9]Blanchard, A., Seraudie, A., Breil, J. F., and Payry, M. J., "Limits of Suction Through a Perforated Metal Sheet on a Model to Avoid Transition Tripping," ONERA-Département d'Études et de Récherches en Aerothermodynamique, Rept. 45/5006.22, Toulouse, France, Oct. 1991.

[10]Goldsmith, J., "Critical Laminar Suction Parameters for Suction into an Isolated Hole or a Single Row of Holes," Northrop Aircraft, Inc., Rept. BLC-95, Hawthorne, CA, Feb. 1957.

[11]Saric, W. S., "Laminar Flow Control with Suction: Theory and Experiment," *Special Course on Aircraft Drag Prediction and Reduction*, AGARD R-723, Aug. 1985, pp. 3.1–3.11.

[12]Gregory, N., "On Critical Suction Conditions for Laminar Boundary-Layer Control by Suction in Perforations," Aeronautical Research Council, Rept. 24,213, 1962.

[13]MacManus, D. G., and Eaton, J. A., "Micro-Scale, Three-Dimensional Navier–Stokes Investigation of a Laminar Flow Control Suction Hole," AIAA Paper 96-0544, Jan. 1996.

[14]MacManus, D. G., Eaton, J. A., Barrett, R. V., and Swales, C., "Three-Dimensional LDV and CFD Studies of the Flow Fields Induced by Suction Through HLFC Perforations," *Proceedings of the 7th International Conference of Laser Anemometry Advances and Applications* (Karlsruhe, Germany), GALA e.V., Karlsruhe, Germany, 1997, pp. 791–798.

[15]MacManus, D. G., "An Aerodynamic Prediction Technique for Laminar Flow Control Suction Surfaces," Ph.D. Thesis, National Univ. of Ireland, Galway, Ireland, Jan. 1997.

[16]Saric, W. S., and Reed, H. L., "Stability and Transition of Three-Dimensional Boundary Layers," *Fluid Dynamics of Three-Dimensional Turbulent Shear Flows and Transition*, CP-438, AGARD, April 1989, pp. 1.1–1.20.

[17]Pfenninger, W., "Laminar Flow Control Laminarization," *Special Course on Concepts for Drag Reduction*, CP-654, AGARD, March 1977, pp. 3.1–3.42.

[18]Saric, W. S., and Yeates, L. G., "Experiments on the Stability of Cross-flow Vortices in Swept-Wing Flows," AIAA Paper 85-0493, Jan. 1985.

[19]Meyer, W., "Preliminary Report on the Flow Field Due to Laminar Suction Through Holes," Northrop Aircraft, Inc., Rept. BLC-75, Hawthorne, CA, March 1955.

[20]MacManus, D. G., and Eaton, J. A., "Measurements and Predictions of the Detailed Flow Induced in a Laminar Boundary Layer by Suction Perforations," *Journal of Fluid Mechanics* (to be published).

[21]Barrett, R. V., Rickards, J., Swales, C., and Brake, C. J., "Enhanced Performance of a Cross-Coupled 3D Laser Doppler Anemometer for Small Scale Flow Surveys Using Improved Alignment and Operational Procedures," *Proceedings of 15th International Congress on Instrumentation in Aerospace Simulation Facilities* (St. Louis, France), ICIASF'93 Record, Inst. of Electrical and Electronics Engineers, New York, 1993, pp. 34.1–34.6.

[22]Bieler, H., and Preist, J., "HLFC for Commercial Aircraft—First ELFIN Test Results," *Proceedings of First European Forum on Laminar Flow Technology* (Hamburg, Germany), DGLR-Bericht 92-06, Deutsche Gesellschaft für Luft- und Raumfahrt, Bonn, Germany, 1992, pp. 193–200.

[23]Rickards, J., "Effect of Suction on the Evolution of Laminar Boundary Layers, Including the Development of Acoustic and LDA Transition Detection Techniques," Ph.D. Thesis, Dept. of Aerospace Engineering, Univ. of Bristol, Bristol, England, UK, Sept. 1994.

[24]MacManus, D. G., Eaton, J. A., Barrett, R., Rickards, J., and Swales, C., "Mapping the Flow Field Induced by a HLFC Perforation Using a High Resolution LDV," AIAA Paper 96-0544, Jan. 1996.

[25]Pearce, W. E., McNay, D. E., and Thelander, J. A., "Laminar Flow Control Leading Edge Glove Flight Test Article Development—Final Report," NASA CR-172137, Nov. 1984.

[26]"Tecplot User's Manual," Amtec Engineering, Inc., Bellevue, WA, 1993.

[27]Reneaux, J., and Blanchard, A., "The Design and Testing of an Airfoil with Hybrid Laminar Flow Control," *Proceedings of First European Forum on Laminar Flow Technology* (Hamburg, Germany), DGLR-Bericht 92-06, Deutsche Gesellschaft für Luft- und Raumfahrt, Bonn, Germany, 1992, pp. 164–174.

[28]Arnal, D., "Boundary Layer Transition: Prediction, Application to Drag Reduction," *Special Course on Skin Friction Drag Reduction*, AGARD R-786, March 1992, pp. 5.1–5.59.

[29]Radeztsky, R., Reibert, M., Saric, W., and Takagi, S., "Effect of Micron-Sized Roughness on Transition in Swept-Wing Flows," AIAA Paper 93-0076, Jan. 1993.

P. R. Bandyopadhyay
Associate Editor

Color reproduction courtesy of Airbus Industrie